

Published in final edited form as:

*J Nucl Med.* 2012 July ; 53(7): 1110–1118. doi:10.2967/jnumed.111.100842.

## PET of EGFR Expression with an $^{18}\text{F}$ -Labeled Affibody Molecule

Zheng Miao, Gang Ren, Hongguang Liu, Shibo Qi, Song Wu, and Zhen Cheng

Molecular Imaging Program at Stanford (MIPS), Bio-X Program, Department of Radiology, Stanford University, Stanford, California

### Abstract

Epidermal growth factor receptor (EGFR) is often overexpressed in a variety of human cancers, and its expression is associated with poor prognosis for many cancer types. However, an accurate technique to noninvasively image EGFR expression in vivo is not available in the clinical setting. In this research, an Affibody analog, anti-EGFR Ac-Cys-Z<sub>EGFR:1907</sub>, was successfully site-specifically  $^{18}\text{F}$ -labeled for PET of EGFR expression.

**Methods**—The prosthetic group *N*-[2-(4- $^{18}\text{F}$ -fluorobenzamido) ethyl] maleimide ( $^{18}\text{F}$ -FBEM) was conjugated to Ac-Cys-Z<sub>EGFR:1907</sub> under mild conditions (pH 7) to produce the probe  $^{18}\text{F}$ -FBEM-Cys-Z<sub>EGFR:1907</sub>. The binding affinity and specificity tests of  $^{18}\text{F}$ -FBEM-Cys-Z<sub>EGFR:1907</sub> to EGFR were conducted using A431 cancer cells. Small-animal PET and biodistribution studies were conducted on various mice tumor xenograft models with EGFR overexpression (6 types) after injection of approximately 2.0 MBq of  $^{18}\text{F}$ -FBEM-Cys-Z<sub>EGFR:1907</sub> with or without coinjection of unlabeled Ac-Cys-Z<sub>EGFR:1907</sub> for up to 3 h after injection. A correlation study between  $^{18}\text{F}$ -FBEM-Cys-Z<sub>EGFR:1907</sub> small-animal PET quantification and ex vivo Western blot analysis of tumor EGFR expression was conducted in those 6 types of tumor models.

**Results**— $^{18}\text{F}$ -FBEM-Cys-Z<sub>EGFR:1907</sub> binds to EGFR with low nanomolar affinity (37 nM) in A431 cells.  $^{18}\text{F}$ -FBEM-Cys-Z<sub>EGFR:1907</sub> rapidly accumulated in the tumor and cleared from most of the normal organs except the liver and kidneys at 3 h after injection, allowing excellent tumor-to-normal tissue contrast to be obtained. In the A431 tumor xenograft model, coinjection of the PET probe with 45  $\mu\text{g}$  of Ac-Cys-Z<sub>EGFR:1907</sub> was able to improve the tumor uptake (3.9 vs. 8.1 percentage of the injected radioactive dose per gram of tissue, at 3 h after injection) and tumor imaging contrast, whereas coinjection with 500  $\mu\text{g}$  of Ac-Cys-Z<sub>EGFR:1907</sub> successfully blocked the tumor uptake significantly (8.1 vs. 1.0 percentage of the injected radioactive dose per gram of tissue, at 3 h after injection, 88% inhibition,  $P < 0.05$ ). Moderate correlation was found between the tumor tracer uptake at 3 h after injection quantified by PET and EGFR expression levels measured by Western blot assay ( $P = 0.007$ ,  $R = 0.59$ ).

**Conclusion**— $^{18}\text{F}$ -FBEM-Cys-Z<sub>EGFR:1907</sub> is a novel protein scaffold-based PET probe for imaging EGFR overexpression of tumors, and its ability to differentiate tumors with high and low EGFR expression in vivo holds promise for future clinical translation.

### Keywords

Affibody; cancer imaging;  $^{18}\text{F}$ ; PET; EGFR

---

Epidermal growth factor receptor 1 (EGFR) is a transmembrane protein belonging to the ErbB receptor kinase family. Overexpression of EGFR has been frequently detected in a

wide range of human tumors, for example, small cell lung cancer, small cell carcinoma of the head and neck, esophageal cancer, gastric cancer, gliomas, colon cancer, pancreas cancer, breast cancer, ovary cancer, bladder cancer, kidney cancer, and prostate cancer (1). Novel drugs such as cetuximab, gefitinib, erlotinib, and lapatinib have shown clinical benefits to head and neck, lung, colorectal, pancreatic, and breast cancer patients by targeting overexpressed or activated EGFR (2–4). Furthermore, the EGFR expression level is a strong prognostic indicator for head and neck, ovarian, cervical, bladder, and esophageal cancers (5,6). EGFR expression level also has moderate prognosis value for breast, colon, gastric, and endometrial cancers. Molecular imaging of EGFR is expected to find many applications, such as prognosis of cancer patients, evaluation of antitumor drug effect, and stratification of cancer patients for molecularly targeted therapy (7).

Affibody (Affibody AB) protein scaffold is based on the Z-domain scaffold derived from 1 of the IgG-binding domains of staphylococcal protein A. Affibody proteins are composed of only 58 amino acid residues, a 3-helix bundle structure. The Affibody molecule libraries can be easily constructed by randomization of 13 amino acid residues in helices 1 and 2 of the 3-helix bundle protein (8–10). Affibody binders with high affinities and specificities against a variety of desired targets, for example, EGFR, human epidermal growth factor receptor type 2 (HER2), and human serum albumin, have been quickly identified (11–14). Subsequently, anti-HER2 Affibody (represented as  $Z_{\text{HER2}}$ ) molecules have been labeled with a variety of radionuclides for imaging of tumors overexpressing HER2 in animal models (15–20). The immunogenicity study has revealed that the  $Z_{\text{HER2}}$  (5 injections at an interval of 3 wk, 20  $\mu\text{g}$  of protein each) does not result in any immunogenicity in rats (21). Recently anti-EGFR Affibody ( $Z_{\text{EGFR}}$ ) proteins have also been labeled with  $^{64}\text{Cu}$  and  $^{111}\text{In}$  for PET and SPECT of EGFR-positive tumors in mice xenografts, respectively (22–26). Furthermore,  $^{111}\text{In}$ - or  $^{68}\text{Ga}$ -labeled  $Z_{\text{HER2}}$  has been successfully and safely used to image 3 breast cancer patients (27). This proof-of-principle clinical study (the first, to our knowledge) on a non-immunoglobulin-based scaffold protein, similar to many preclinical studies, clearly demonstrates that Affibody molecules are a promising new class of cancer-targeting ligands with high clinical translation ability and thus worthy of further investigation to develop probes to image different tumor targets.

In our previous research, anti-EGFR Affibody-based molecular probes,  $^{64}\text{Cu}$ -DOTA-Cys- $Z_{\text{EGFR}:1907}$  and Cy5.5-Cys- $Z_{\text{EGFR}:1907}$ , were successfully prepared and found to show rapid tumor targeting ability and good tumor imaging contrast even at 1 h after injection in the EGFR-expressing A431 tumor xenograft model (24,28). These results suggest that the relatively small size of Affibody proteins generally leads to fast clearance rate, quick tumor accumulation, and a relatively short in vivo biologic half-life, which matches well with the physical half-life of  $^{18}\text{F}$  (110 min, emits positron ( $\beta^+$ ) particles at a maximum energy of 635 keV and average energy of 250 keV, 97% abundance), one of the most widely used PET radioisotopes in nuclear medicine clinics. Therefore, in this study, to further develop an anti-EGFR Affibody-based probe for future clinical translation, Ac-Cys- $Z_{\text{EGFR}:1907}$  was site-specifically labeled with  $^{18}\text{F}$  by site-specific conjugation with the prosthetic group *N*-[2-(4- $^{18}\text{F}$ -fluorobenzamido) ethyl] maleimide ( $^{18}\text{F}$ -FBEM), through the N terminus cysteine residue (Fig. 1) (29). The resulting probe,  $^{18}\text{F}$ -FBEM-Cys- $Z_{\text{EGFR}:1907}$ , was then evaluated in a variety of tumor models (A431, SAS, SQ20B, 22B, U87MG, and HT29) to study whether

the PET probe can be used for imaging of EGFR-positive tumors and quantitative PET of EGFR expression in vivo.

## MATERIALS AND METHODS

### Chemistry and Radiochemistry

The Affibody molecule Ac-Cys-Z<sub>EGFR:1907</sub> (Ac-CVDNKFNK-EMWAAWEEIRNLPNLNGWQMTAFIASLVDDPSQSANLLAE-AKKLNDAQAPK-NH<sub>2</sub>) was synthesized on a CS Bio CS336 instrument using a previously reported synthesis method (24,28). Purified peptide was dissolved in water, and concentration was determined by amino acid analysis (Molecular Structure Facility). Peptide purity and molecular mass were determined by analytic scale reversed-phase high-performance liquid chromatography (RP-HPLC) and matrix-assisted laser desorption/ionization–time of flight mass spectrometry (MALDI-TOF-MS) or electrospray ionization mass spectrometry. Nonradioactive <sup>19</sup>F-FBEM-Cys-Z<sub>EGFR:1907</sub>, a reference standard, was prepared by reaction of Ac-Cys-Z<sub>EGFR:1907</sub> with FBEM. Briefly, Ac-Cys-Z<sub>EGFR:1907</sub> (0.07 μmol, 0.5 mg in 500 μL of sodium acetate buffer, pH 6.0, with 0.1% ascorbic acid) was mixed with 1.5 μmol of FBEM (0.36 mg in 100 μL of dimethyl sulfoxide) and reacted for 1 h at room temperature. The resulting conjugate, <sup>19</sup>F-FBEM-Cys-Z<sub>EGFR:1907</sub>, was then purified by RP-HPLC on a semipreparative C<sub>18</sub> column (Luna; Phenomenex) using a gradient system of solvent A (0.1% trifluoroacetic acid [TFA]/H<sub>2</sub>O) and solvent B (0.1% TFA/acetonitrile). The flow rate was 3 mL/min, with the mobile phase starting from 90% solvent A and 10% solvent B (0–3 min) to 35% solvent A and 65% solvent B at 33 min. Fractions containing the product were collected and lyophilized. The identity of <sup>19</sup>F-FBEM-Cys-Z<sub>EGFR:1907</sub> was confirmed by MALDI-TOF-MS.

The prosthetic group <sup>18</sup>F-FBEM was prepared by reaction of the *N*-succinimidyl-4-<sup>18</sup>F-fluorobenzoate (<sup>18</sup>F-SFB) with aminoethyl-maleimide (Fig. 1). First, <sup>18</sup>F-SFB was prepared on the basis of a recent reported procedure (30). Then <sup>18</sup>F-SFB in 100 μL of dimethyl sulfoxide was added to amino-ethyl-maleimide (1.5 mg, in 100 μL of dimethyl sulfoxide) and 25 μL of diisopropylethylamine and reacted for 30 min at 50°C. After the addition of 30 μL of TFA to quench the reaction, the mixture was purified with the semipreparative HPLC, using the same elution gradient as for the cold FBEM purification. The eluted fractions containing the <sup>18</sup>F-FBEM were then collected, combined, and dried using a rotary evaporator. Then <sup>18</sup>F-FBEM was resuspended with 300 μL of NaOAc (0.1 M, 0.1% ascorbic acid, pH 7), and 100 μg of Ac-Cys-Z<sub>EGFR:1907</sub> was added to the solution and incubated at room temperature for 40 min. The reaction solution was passed through a PD-10 column, and the radiolabeled product, <sup>18</sup>F-FBEM-Cys-Z<sub>EGFR:1907</sub>, was eluted out with phosphate-buffered saline (PBS) (0.01 M, pH 7.4) and passed through a 0.22-μm Millipore filter into a sterile vial for cell culture and animal experiments. The radiochemical purity of <sup>18</sup>F-FBEM-Cys-Z<sub>EGFR:1907</sub> was then analyzed by the RP-HPLC equipped with a radioactive detector (radio-HPLC).

## Cell Culture

Epithelial cancer (A431), head and neck cancer (SQ20B, SAS, and 22B), colon cancer (HT29), and glioma cancer (U87MG) cells were cultured in Dulbecco modified Eagle medium containing high glucose (Gibco), which was supplemented with 10% fetal bovine serum and 1% penicillin–streptomycin. The cells were expanded in tissue culture dishes and kept in a humidified atmosphere of 5% CO<sub>2</sub> at 37°C. The medium was changed every other day. A confluent monolayer was detached with 0.5% trypsin-ethylenediaminetetraacetic acid, PBS (0.01 M, pH 7.4), and dissociated into a single-cell suspension for further cell culture and assays.

For the fluorescence microscopy study of ligand displacement, EGFR–high-expression A431 and SAS cells ( $1 \times 10^5$ ) were cultured on the 35-mm MatTek glass bottom culture dishes. After 24 h, the cells were washed with PBS and then incubated at 37°C with Cy5.5-labeled epidermal growth factor (Cy5.5-EGF, 150 nM) for 1 h in the dark (31). EGFR binding specificity of Ac-Cys-Z<sub>EGFR:1907</sub> in cell culture was verified by incubating the A431 and SAS cells with or without large amounts of (blocking dose) Ac-Cys-Z<sub>EGFR:1907</sub> (10 μM). After the incubation period, cells were washed 3 times with ice-cold PBS. The fluorescence signal of the cells was recorded using an Axiovert 200 M fluorescence microscope (Carl Zeiss MicroImaging, Inc.) equipped with a Cy5.5 filter set (exciter, HQ 650/20 nm; emitter, HQ 695/35 nm). An AttoArc HBO 100W microscopic illuminator was used as a light source for fluorescence excitation. Images were taken using a thermoelectrically cooled charge-coupled device (CCD) (Micromax, model RTE/CCD-576; Princeton Instruments Inc.) and analyzed using MetaMorph software (version 6.2r4; Molecular Devices Corp.).

The receptor saturation assay of <sup>18</sup>F-FBEM-Cys-Z<sub>EGFR:1907</sub> was conducted with the EGFR–high-expression A431 cells. The cells ( $3 \times 10^5$ ) were plated on 6-well plates 1 d before the experiment. Cells were washed with PBS 3 times. Serum-free Dulbecco modified Eagle medium (1 mL) was added to each well. The probe (8.9–532.8 kBq [0.24–14.4 μCi], 2–120 nM final concentration) with or without 100 times excess of Ac-Cys-Z<sub>EGFR:1907</sub> was added to the wells. After the plates were put on ice for 2 h, the cells were washed with cold PBS 3 times and detached with TrypLE-Express (Invitrogen). The radioactivity of the cells was measured using a γ-counter. The data were analyzed using GraphPad Prism (GraphPad Software, Inc.), and the dissociation constant (K<sub>D</sub>) of the <sup>18</sup>F-FBEM-Cys-Z<sub>EGFR:1907</sub> was calculated from a 1-site-fit binding curve.

## In Vitro and In Vivo Stability

<sup>18</sup>F-FBEM-Cys-Z<sub>EGFR:1907</sub> (1.85–7.4 MBq [50–200 μCi]) was incubated in 0.5 mL of mouse serum for various times (1 or 3 h) at 37°C. At each time point, the mixture was resuspended in 0.5 mL of acetonitrile and centrifuged at 16,000g for 2 min. The supernatant containing greater than 95% of the radioactivity was filtered using a 0.2-μm nylon SpinX column (Corning Inc.). Greater than 99% of the radioactivity passed through this filter. The samples were analyzed by radio-HPLC, and the percentage of intact PET probe was determined by quantifying peaks corresponding to the intact probe and to the degradation products.

In vivo stability was determined with a procedure similar to one described previously (32). Briefly, nude mice bearing A431 tumors were injected with  $^{18}\text{F}$ -FBEM-Cys-Z<sub>EGFR:1907</sub> (11.1 MBq [300  $\mu\text{Ci}$ ]) via the tail vein and euthanized at 1 h after injection. The tumor was removed and homogenized with dimethylformamide (0.5 mL) with 1% Triton X-100 (Sigma-Aldrich). A blood sample was centrifuged immediately after collection to remove the blood cells. The plasma portion was added with dimethylformamide (0.5 mL) with 1% Triton X-100. After centrifugation, the supernatant portion was diluted with solution A (99.9% H<sub>2</sub>O with 0.1% TFA) and centrifuged again at 16,000g for 2 min with a nylon filter. The filtrate was analyzed by radio-HPLC under conditions identical to those used for analyzing the original radiolabeled peptide. Eluted fractions were collected every 30 s; the radioactivity of each fraction was measured with a  $\gamma$ -counter, and the resulting radio-HPLC chromatogram was plotted.

### Animal Xenograft Model

All animal studies were performed in compliance with federal and local institutional rules for the conduct of animal experimentation. Approximately  $5 \times 10^6$  cultured A431, SQ20B, SAS, 22B, HT29, and U87MG cells were suspended in PBS/Matrigel (1:1) (BD Bioscience) or PBS alone (for A431) and subcutaneously implanted in the right shoulders of nude mice. Tumors were allowed to grow to 0.5–1.0 cm in diameter (3–6 wk) before imaging experiments.

For biodistribution studies, A431 tumor-bearing mice ( $n = 3$  or 4 for each group) were injected with  $^{18}\text{F}$ -FBEM-Cys-Z<sub>EGFR:1907</sub> (1.9–2.6 MBq [50–70  $\mu\text{Ci}$ ], 2–3  $\mu\text{g}$ ) spiked with 0 or 45  $\mu\text{g}$  of unlabeled Ac-Cys-Z<sub>EGFR:1907</sub> via the tail vein. Then mice were sacrificed at 3 or 2 h after injection for  $^{18}\text{F}$ -FBEM-Cys-Z<sub>EGFR:1907</sub>, respectively. Moreover, tumor mice (SQ20B, SAS, 22B, HT29, and U87MG,  $n = 3$  for each tumor model) were also injected with  $^{18}\text{F}$ -FBEM-Cys-Z<sub>EGFR:1907</sub> (1.9–2.6 MBq [50–70  $\mu\text{Ci}$ ], 2–3  $\mu\text{g}$ ) spiked with 45  $\mu\text{g}$  of unlabeled Ac-Cys-Z<sub>EGFR:1907</sub> via the tail vein. At 3 h after injection, mice were sacrificed and tumor and normal tissues of interest were removed and weighed and their radioactivity was measured with a  $\gamma$ -counter. The radioactivity uptake in the tumor and normal tissues was expressed as a percentage injected radioactive dose per gram of tissue (%ID/g). For testing of the in vivo EGFR-targeting specificity of  $^{18}\text{F}$ -FBEM-Cys-Z<sub>EGFR:1907</sub>, nude mice bearing A431 tumors ( $n = 3$ ) were also coinjected the probe (300  $\mu\text{g}$  of Ac-Cys-Z<sub>EGFR:1907</sub>) via the tail vein, and biodistribution at 3 h after injection was examined.

### Small-Animal PET

Mice bearing A431 xenografts were injected with approximately 1.9–2.6 MBq (50–70  $\mu\text{Ci}$ ) of  $^{18}\text{F}$ -FBEM-Cys-Z<sub>EGFR:1907</sub> spiked with 0, 45, or 500  $\mu\text{g}$  of unlabeled Ac-Cys-Z<sub>EGFR:1907</sub> via the tail vein, and PET was performed using a small-animal PET R4 rodent model scanner (Siemens Medical Solutions USA, Inc.). At 1, 2, and 3 h after injection, mice were anesthetized with isoflurane (5% for induction and 2% for maintenance in 100% O<sub>2</sub>). Between each scan, mice were woken up to empty the bladder. With the help of a laser beam attached to the scanner, mice were placed prone and near the center of the field of view of the scanner, and 3-min static scans were obtained. For the correlation study, mice bearing SAS, SQ20B, 22B, U87MG, and HT29 xenograft tumors were injected with approximately

1.85–2.59 MBq (50–70  $\mu\text{Ci}$ ) of  $^{18}\text{F}$ -FBEM-Cys-Z<sub>EGFR:1907</sub> spiked with 45  $\mu\text{g}$  of Ac-Z<sub>EGFR:1907</sub> via the tail vein. Small-animal PET was conducted at 1, 2, and 3 h after injection. At 3 h after injection, mice were sacrificed, and the biodistribution study was performed as described. All the small-animal PET images were reconstructed by a 2-dimensional ordered-subsets expectation maximization algorithm. No background correction was performed. Region of interests (ROIs) (5 pixels for coronal and transaxial slices) were drawn over the tumor on decay-corrected whole-body coronal images. Values in 3–10 adjacent slices (depending on the size of the tissue or organ) were averaged to obtain a reproducible value of radioactivity concentration. The maximum counts per pixel per minute were obtained from the ROIs and were converted to counts per milliliter per minute using a calibration constant. ROIs were then converted to counts per gram per minute based on the assumption of a tissue density of 1 g/mL, and image ROI-derived %ID/g values were determined by dividing counts per gram per minute by injected dose. No attenuation correction was performed.

### Western Blot and Correlation Study

After the small-animal PET studies and radioactivity had mostly decayed, the mice were sacrificed and the tumor tissues were harvested. Tumor tissue was extracted using radioimmunoprecipitation assay tissue protein extraction buffer, and the concentration was determined using microBCA protein assay kit (Pierce Biotechnology, Inc.). After sodium dodecyl sulfate polyacrylamide gel electrophoresis separation of 30  $\mu\text{g}$  of total protein, the protein was transferred to a polyvinylidene fluoride membrane (Invitrogen Corp.) and incubated at room temperature with 5% nonfat milk blocking buffer. The blots were then incubated overnight at 4°C with anti-EGFR antibody (Cell Signaling Technology), followed by incubation at room temperature for 1 h with horseradish peroxidase-conjugated antihuman antibody (GE Healthcare). The bands were detected using the ECL Western blotting detection system (GE Healthcare). Actin was used as a loading control. After development, films were scanned with a scanner using gray-scale mode. The images were opened in ImageJ, a Java-based image-processing software. Background signal was subtracted before normalization. Three samples of each tumor model (except A431,  $n = 4$ ) were prepared for Western blot to obtain semiquantitative data for statistical analysis.

### Statistical Method

Statistical analysis was performed using the 2-tailed Student *t* test for unpaired data. A 95% confidence level was chosen to determine the significance between groups, with a *P* value less than 0.05 being designated as indicating a significant difference. Correlation was conducted on GraphPad Prism with the best-fit linear regression line, with a *P* value less than 0.05 being designated as indicating a correlation.

## RESULTS

### Chemistry and Radiochemistry

Ac-Cys-Z<sub>EGFR:1907</sub> was conjugated with amino-ethylmaleimide to prepare the nonradioactive 19F-FBEM-Cys-Z<sub>EGFR:1907</sub>, which can be used as a reference for characterization of radiolabeled peptide, and the product was purified by a C4 analytic



HPLC. MS analysis of the final product only showed the expected mass peak for  $^{19}\text{F}$ -FBEM-Cys-Z<sub>EGFR:1907</sub>. The measured molecular weight was  $m/z = 6,950$  for  $[\text{M}+\text{H}]^+$  (calculated molecular weight  $[\text{M}+\text{H}]^+ = 6,950.2$ ). The recovery yield was 80% after purification, and the purity for the final product was over 95% (retention time, 28 min).

Similarly,  $^{18}\text{F}$ -FBEM-Cys-Z<sub>EGFR:1907</sub> was synthesized by coupling Ac-Cys-Z<sub>EGFR:1907</sub> with prosthetic group  $^{18}\text{F}$ -FBEM. Radiosynthesis and purification of  $^{18}\text{F}$ -FBEM-Cys-Z<sub>EGFR:1907</sub> were completed in approximately 3 h. The maximum overall radiochemical yield with decay correction was 10% at the end of synthesis. The radiochemical purity of the labeled peptide was over 95% as verified by analytic HPLC analysis, with a specific activity of approximately 10 GBq/ $\mu\text{mol}$ .

### In Vitro Cell Binding Assay

The binding specificity and affinity were measured in vitro using A431 cells. Blocking with a large amount of Ac-Cys-Z<sub>EGFR:1907</sub> efficiently reduced the Cy5.5-EGF uptake by EGFR-positive cells (Fig. 2A), supporting the specific binding of Ac-Cys-Z<sub>EGFR:1907</sub> to EGFR. Moreover, binding specificity and affinity also demonstrate that the anti-EGFR Affibody molecule Ac-Cys-Z<sub>EGFR:1907</sub> probably shares the same binding pocket as that of the Cy5.5-EGF or these 2 molecules bind to regions close to each other on the receptor surface. The relative binding affinity of  $^{18}\text{F}$ -FBEM-Cys-Z<sub>EGFR:1907</sub> to cell surface receptors was determined through receptor saturation assay. The mean  $\pm$  SD of  $K_D$  values of  $^{18}\text{F}$ -FBEM-Cys-Z<sub>EGFR:1907</sub> is  $37 \pm 3$  nM (Fig. 2B), which is similar to that of DOTA-Cys-Z<sub>EGFR:1907</sub> ( $K_D$ , 20 nM) and Cy5.5-Cys-Z<sub>EGFR:1907</sub> ( $K_D$ , 44 nM). These studies suggest that conjugation of  $^{18}\text{F}$ -FBEM moiety to the N terminus of Affibody Z<sub>EGFR:1907</sub> through cysteine residue largely maintain its EGFR binding affinity.

### In Vitro Stability and Metabolite Analysis

To test serum stability, purified  $^{18}\text{F}$ -FBEM-Cys-Z<sub>EGFR:1907</sub> (50  $\mu\text{L}$ ) was incubated in 500  $\mu\text{L}$  of mouse serum at 37°C, and radio-HPLC analysis indicated that more than 90% of the probe remained intact during 1- to 3-h incubation (Figs. 3A and 3B). Next, the in vivo stability of  $^{18}\text{F}$ -FBEM-Z<sub>EGFR:1907</sub> was determined using samples recovered from the tumor and plasma of A431 tumor mice injected with the probe. In plasma and tumor, 85% and 95%, respectively, of the probe remained intact at 1 h after injection (Figs. 3C and 3D). These studies demonstrate the excellent stability of  $^{18}\text{F}$ -FBEM-Cys-Z<sub>EGFR:1907</sub>, which provides the solid foundation for quantitative imaging of EGFR expression in vivo using this PET probe.

### Biodistribution Studies

The in vivo biodistribution of  $^{18}\text{F}$ -FBEM-Cys-Z<sub>EGFR:1907</sub> was next determined in mice bearing A431 xenografts at 3 h after injection (Table 1).  $^{18}\text{F}$ -FBEM-Cys-Z<sub>EGFR:1907</sub> displayed high accumulation in A431 tumors ( $3.94 \pm 0.39$  % ID/g at 3 h after injection). Kidney and liver uptake was  $3.78 \pm 0.36$  and  $9.28 \pm 1.61$  % ID/g, respectively. Lower levels of radioactivity were observed in blood ( $1.32 \pm 0.07$  % ID/g) and most other organs. For the in vivo blocking study,  $^{18}\text{F}$ -FBEM-Cys-Z<sub>EGFR:1907</sub> was coinjected with a large excess (500  $\mu\text{g}$ ) of the unlabeled Ac-Cys-Z<sub>EGFR:1907</sub> to saturate endogenous and overexpressed EGFR.

The coinjection of Ac-Cys-Z<sub>EGFR:1907</sub> specifically reduced the tumor uptake of <sup>18</sup>F-FBEM-Cys-Z<sub>EGFR:1907</sub> from  $3.94 \pm 0.39$  to  $0.97 \pm 0.42$  %ID/g at 3 h after injection (75% inhibition,  $P < 0.05$ ), whereas the liver uptake also decreased from  $9.28 \pm 1.61$  to  $0.33 \pm 0.15$  (96% inhibition,  $P < 0.05$ ). Kidney uptake is not significantly changed in the blocking group ( $3.78 \pm 0.36$  vs.  $6.14 \pm 2.87$ ,  $P > 0.05$ ). Interestingly, coinjection with a moderate dose of cold Ac-Cys-Z<sub>EGFR:1907</sub> (45 μg) dramatically enhanced the tumor uptake of <sup>18</sup>F-FBEM-Cys-Z<sub>EGFR:1907</sub> by nearly 1-fold ( $8.06 \pm 1.44$  vs.  $3.94 \pm 0.39$ ,  $P < 0.05$ ), with increased tumor-to-all-normal-organ ratios at 3 h after injection.

A biodistribution study of <sup>18</sup>F-FDG in the A431 tumor model was also performed at 2 h after injection. <sup>18</sup>F-FDG showed high tumor uptake and a high tumor-to-blood ratio, but tumor-to-muscle and tumor-to-lung ratios were significantly lower than that of <sup>18</sup>F-FBEM-Cys-Z<sub>EGFR:1907</sub> coinjected with 45 μg of cold Ac-Cys-Z<sub>EGFR:1907</sub> (Table 1) ( $P < 0.05$ ).

<sup>18</sup>F-FBEM-Cys-Z<sub>EGFR:1907</sub> was further evaluated in several EGFR overexpression tumor xenograft models, and biodistribution was performed at 3 h after injection. <sup>18</sup>F-FBEM-Cys-Z<sub>EGFR:1907</sub> displayed moderate to high tumor uptake (1.0–4.8 %ID/g) in HT29, U87MG, SQ20B, 22B, and SAS models (Fig. 4A). Uptake of the PET probe in all other organs and blood were also low except in the kidneys, lung, and liver.

### Small-Animal PET

The in vivo tumor targeting and imaging profile of <sup>18</sup>F-FBEM-Cys-Z<sub>EGFR:1907</sub> was further investigated in A431 tumor-bearing nude mice by static small-animal PET at 1 and 3 h after tail vein injection of 1.9–2.6 MBq (50–70 μCi) of <sup>18</sup>F-FBEM-Cys-Z<sub>EGFR:1907</sub>.

Representative decay-corrected coronal small-animal PET images of nude mice bearing A431 tumors on their right shoulder at 1 and 3 h after injection are shown in Figure 5. The A431 tumor was clearly delineated with good tumor-to-contralateral-background contrast at 1 and 3 h after injection (left and right images in Fig. 5). Moreover, the coinjection of 45 μg of Ac-Cys-Z<sub>EGFR:1907</sub> increased the tumor uptake of <sup>18</sup>F-FBEM-Cys-Z<sub>EGFR:1907</sub>, resulting in higher tumor-to-background contrast at all time points (middle images in Fig. 5). Finally, when coinjected with 500 μg of Ac-Cys-Z<sub>EGFR:1907</sub>, tumor was barely visible. The dynamic PET scans showed that most <sup>18</sup>F-FBEM-Cys-Z<sub>EGFR:1907</sub> was quickly cleared through the renal-urine system, and the blood uptake dropped dramatically in the first 35 min after injection (Supplemental Fig. 1; supplemental materials are available online only at <http://jnm.snmjournals.org>). Small-animal PET of several EGFR-positive tumors also revealed rapid tumor targeting and accumulation of <sup>18</sup>F-FBEM-Cys-Z<sub>EGFR:1907</sub> as early as 1 h after injection (Fig. 4B).

### Correlation Study

Quantitative analysis of small-animal PET images at 1 and 3 h after injection was performed to obtain mean or maximum organ uptake such as tumor and liver uptake of <sup>18</sup>F-FBEM-Cys-Z<sub>EGFR:1907</sub>. The tumor uptake or tumor-to-liver uptake ratios at different time points were then plotted against the relative EGFR expression levels measured by Western blot (normalized against actin protein) (Fig. 6A). The plots revealed that at 1 h after injection, there was a poor correlation between small-animal PET and Western assay (mean %ID/g vs.



EGFR level,  $R = 0.37$ ,  $P = 0.120$ ), whereas at 3 h after injection, there was a moderate correlation (mean %ID/g vs. EGFR level,  $R = 0.59$ ,  $P = 0.007$ ) (Figs. 6B and 6C). A moderate correlation was achieved when the tumor-to-liver ratio (mean %ID/g of  $^{18}\text{F}$ -FBEM-Cys- $Z_{\text{EGFR}:1907}$  at 3 h after injection) was used for analysis ( $R = 0.66$ ,  $P = 0.002$ ) (Fig. 6D).

## DISCUSSION

Novel nonimmunogenic small protein scaffolds such as Affibody molecules have drawn a lot of attention for the development of cancer molecular imaging probes and therapeutics, because of their easy synthesis, possibility for site-specific labeling, stable structure, and high versatility targeting of various cancer biomarkers. In this research, we thus prepared the  $^{18}\text{F}$ -FBEM-labeled Ac-Cys- $Z_{\text{EGFR}:1907}$  (Fig. 1) to develop a PET probe that had high potential for imaging EGFR expression in clinics.

Considering the short physical half-life of  $^{18}\text{F}$  and the relatively short biologic blood half-life of the Affibody, biodistribution and imaging studies of  $^{18}\text{F}$ -FBEM-Cys- $Z_{\text{EGFR}:1907}$  were acquired in a short time frame (up to 3 h after injection). Consistent with our expectation, because of the excellent tumor targeting and retention ability of Affibody molecules and their rapid blood clearance, excellent tumor imaging quality of  $^{18}\text{F}$ -FBEM-Cys- $Z_{\text{EGFR}:1907}$  was observed in EGFR-positive tumors, especially in tumors with high and moderate EGFR expression levels (Fig. 4). For example, the A431 tumor is clearly delineated from normal tissue at both 1 and 3 h after injection. Quantification of small-animal PET images shows that 80% of the activity remains in the tumor at 3 h after injection, compared with the uptake at 1 h. PET and biodistribution show that at 3 h after injection, the A431 tumor uptake of  $^{18}\text{F}$ -FBEM-Cys- $Z_{\text{EGFR}:1907}$  (spiked with 45  $\mu\text{g}$  of Ac-Cys- $Z_{\text{EGFR}:1907}$ ) can even achieve approximately 8 %ID/g (Table 1). Interestingly, quantification also found that the tumor-to-background contrasts of the  $^{18}\text{F}$ -FBEM-Cys- $Z_{\text{EGFR}:1907}$  can be improved significantly with the increase of time (1–3 h). In addition, coinjection with 45  $\mu\text{g}$  of Affibody dramatically increased the tumor uptake and the imaging quality. The tumor-to-blood ratio also increased from 1.05 to 2.58 at 0.5 h (Table 1). These results are in sharp contrast with the slow accumulation and tumor imaging properties of monoclonal antibody-based probes, which generally display a tumor-to-blood ratio of only 0.5 at 1 d and 1.5 at 4 d after injection of the probe in a A431 xenograft model (33,34). Finally, the tumor uptake can be specifically blocked by the large dose of cold Affibody, proving the *in vivo* tumor-targeting specificity of  $^{18}\text{F}$ -FBEM-Cys- $Z_{\text{EGFR}:1907}$ .

On the basis of the imaging and biodistribution study,  $^{18}\text{F}$ -FBEM-Cys- $Z_{\text{EGFR}:1907}$  exhibits rather low accumulations in most normal organs. Although the kidney and liver show the highest uptake because they are the major organs of metabolism, and the liver also has high expression level of EGFR (24). Dynamic scanning of  $^{18}\text{F}$ -FBEM-Cys- $Z_{\text{EGFR}:1907}$  coinjected with 45  $\mu\text{g}$  of Ac-Cys- $Z_{\text{EGFR}:1907}$  reveals rapid clearance of the probe from the blood in the first 35 min after injection. The kidney uptake reaches a peak at about 20 min and rapidly decreases after that (Supplemental Fig. 1). Biodistribution verifies that  $^{18}\text{F}$ -FBEM-Cys- $Z_{\text{EGFR}:1907}$ , compared with radiometal-labeled  $Z_{\text{EGFR}:1907}$ , exhibits significantly reduced accumulation in the kidneys (~200 %ID/g vs. 4 %ID/g at 3 h). Even in the liver,  $^{18}\text{F}$ -FBEM-

Cys-Z<sub>EGFR:1907</sub> displays only around 6 % ID/g at 3 h after injection, which is much lower than with <sup>64</sup>Cu-labeled DOTA-Z<sub>EGFR:1907</sub> (13.3 % ID/g at 4 h) (35), allowing the possibility of the detection of tumor metastasis in the abdomen region. Moreover, low radioactivity was found in the lung region. This result is in agreement with previous data indicating that the normal lung tissue expresses low EGFR (1). The low uptake of <sup>18</sup>F-FBEM-Cys-Z<sub>EGFR:1907</sub> in the lung region offers considerable advantages for this PET probe to identify primary or metastatic lung tumors expressing EGFR. Low activity was also observed in the brain (Table 1), suggesting that <sup>18</sup>F-FBEM-Cys-Z<sub>EGFR:1907</sub> does not behave like epidermal growth factor (EGF) and cannot penetrate through the blood–brain barrier. However, <sup>18</sup>F-FBEM-Cys-Z<sub>EGFR:1907</sub> could potentially be used for imaging of glioma because it often overexpresses EGFR and the blood–brain barrier could be disrupted. Overall, these results suggest <sup>18</sup>F-FBEM-Cys-Z<sub>EGFR:1907</sub> possesses excellent pharmacokinetics and is suitable for in vivo imaging of EGFR-positive tumor and EGFR expression.

It is well known that EGFR phosphorylation caused by ligand stimulation or dimerizations with other EGFR family proteins such as HER2 could trigger much downstream signaling of cell proliferation, apoptosis, and metastasis (3,6). Thus, EGFR expression level has a prognostic value except in a few cancers, such as non–small cell lung cancer, for which EGFR mutation is more significant (36,37). <sup>131</sup>I-labeled small protein recombinant human EGF has been successfully used to image lung cancer in a clinical study (38). However, human EGF is not an ideal protein scaffold for PET probe development because of the potent biologic effect of EGF when a large amount of the protein is administered in a short time (>10 µg/h) (38). Our results show that Ac-Cys-Z<sub>EGFR:1907</sub> competes with EGF for the same binding pocket of EGFR, and it also did not cause any toxicity to the A431 and SAS cells at even 10 µM (Fig. 2A). Considering that the anti-HER2 Affibody has been safely used in the clinic for imaging of patients with PET and SPECT (40), Ac-Cys-Z<sub>EGFR:1907</sub>–based molecular probes such as <sup>18</sup>F-FBEM-Cys-Z<sub>EGFR:1907</sub> are likely to have high clinical translation ability.

<sup>18</sup>F-FBEM-Cys-Z<sub>EGFR:1907</sub> shows excellent in vivo stability and stays almost intact in the tumor and blood at 1 h after injection (>90% fraction), warranting its use for the imaging of EGFR expression. However, this probe also has a slightly high blood-pool uptake (at 3 h after injection, >3 % ID/g, Table 1); thus, highly vascularized tumors could show better tumor PET quality because more <sup>18</sup>F-FBEM-Cys-Z<sub>EGFR:1907</sub> is nonspecifically perfused and trapped inside the tumor at early time points after injection. Therefore, at 1 h after injection, there is a poor correlation between tumor uptake and EGFR expression level ( $P = 0.120$  and  $0.086$  using mean and maximum value of uptake, respectively) (Fig. 6B; Supplemental Fig. 2A). However, at 3 h after injection, a moderate correlation between <sup>18</sup>F-FBEM-Cys-Z<sub>EGFR:1907</sub> PET quantification and EGFR protein expression was observed (mean,  $R = 0.59$ ,  $P = 0.007$ ; tumor to liver,  $R = 0.66$ ,  $P = 0.002$ ) using a few types of EGFR-positive tumor models. Uptake of <sup>18</sup>F-FBEM-Cys-Z<sub>EGFR:1907</sub> by tumors with high EGFR expression (A431, SQ20B, and SAS) is higher than that by tumors with low EGFR expression (U87MG, HT29, and 22B). Other factors that affect uptake of <sup>18</sup>F-FBEM-Cys-Z<sub>EGFR:1907</sub>, such as different tumor vascularity and necrosis, could potentially be corrected by <sup>15</sup>O-water blood flow testing and multimodality PET/CT and PET/MRI.

In addition, even though the binding affinity of  $^{18}\text{F}$ -FBEM-Cys-Z<sub>EGFR:1907</sub> is lower than that of many monoclonal antibody-based probes (usually in single-digit nanomolar affinity), the binding affinity could be improved by maturation of EGFR Affibody and multimerization of Affibody (21,25). The pharmacokinetics could also be further improved using linkers or different  $^{18}\text{F}$ -labeling approaches such as PEGylation and  $^{18}\text{F}$ -AIF radiolabeling (39,40).

## CONCLUSION

Anti-EGFR Affibody Ac-Cys-Z<sub>EGFR:1907</sub> was for the first time, to our knowledge, successfully site-specifically radio-labeled with  $^{18}\text{F}$ .  $^{18}\text{F}$ -FBEM-Cys-Z<sub>EGFR:1907</sub> shows favorable in vivo profiles and excellent tumor imaging quality. Ac-Cys-Z<sub>EGFR:1907</sub> is a promising PET probe for imaging EGFR-positive tumors and EGFR expression level. It has high clinical translational ability and will likely find broad applications in EGFR-targeted patient therapy and management.

## Supplementary Material

Refer to Web version on PubMed Central for supplementary material.

## Acknowledgments

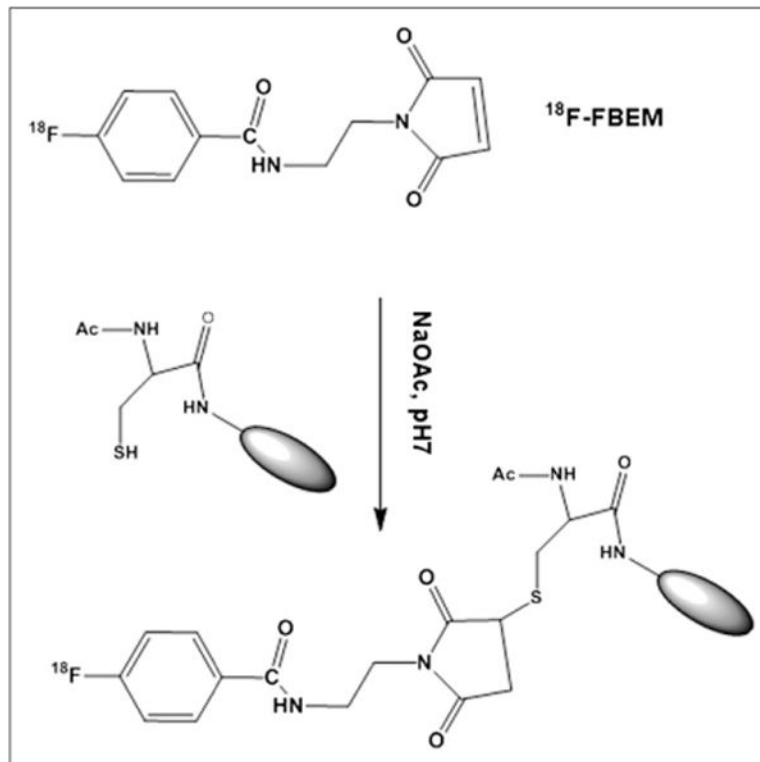
We thank Dr. Frederick Chin and the team at the radiochemistry facility for  $^{18}\text{F}$  production. This work was supported, in part, by the Department of Radiology, Stanford University, and the National Cancer Institute (NCI) 5R01 CA119053. No other potential conflict of interest relevant to this article was reported.

## References

1. Real FX, Rettig WJ, Chesa PG, Melamed MR, Old LJ, Mendelsohn J. Expression of epidermal growth factor receptor in human cultured cells and tissues: relationship to cell lineage and stage of differentiation. *Cancer Res.* 1986; 46:4726–4731. [PubMed: 3015394]
2. Burris HA 3rd. Dual kinase inhibition in the treatment of breast cancer: initial experience with the EGFR/ErB-2 inhibitor lapatinib. *Oncologist.* 2004; 9(suppl 3):10–15. [PubMed: 15163842]
3. Geyer CE, Forster J, Lindquist D, et al. Lapatinib plus capecitabine for HER2-positive advanced breast cancer. *N Engl J Med.* 2006; 355:2733–2743. [PubMed: 17192538]
4. Jones HE, Goddard L, Gee JM, et al. Insulin-like growth factor-I receptor signalling and acquired resistance to gefitinib (ZD1839; Iressa) in human breast and prostate cancer cells. *Endocr Relat Cancer.* 2004; 11:793–814. [PubMed: 15613453]
5. DiGiovanna MP, Stern DF, Edgerton SM, Whalen SG, Moore D 2nd, Thor AD. Relationship of epidermal growth factor receptor expression to ErbB-2 signaling activity and prognosis in breast cancer patients. *J Clin Oncol.* 2005; 23:1152–1160. [PubMed: 15718311]
6. Nicholson RI, Gee JM, Harper ME. EGFR and cancer prognosis. *Eur J Cancer.* 2001; 37(suppl 4):S9–S15. [PubMed: 11597399]
7. Pantaleo MA, Nannini M, Maleddu A, et al. Experimental results and related clinical implications of PET detection of epidermal growth factor receptor (EGFr) in cancer. *Ann Oncol.* 2009; 20:213–226. [PubMed: 18842614]
8. Miao Z, Levi J, Cheng Z. Protein scaffold-based molecular probes for cancer molecular imaging. *Amino Acids.* 2011; 41:1037–1047. [PubMed: 20174842]
9. Nilsson FY, Tolmachev V. Affibody molecules: new protein domains for molecular imaging and targeted tumor therapy. *Curr Opin Drug Discov Devel.* 2007; 10:167–175.

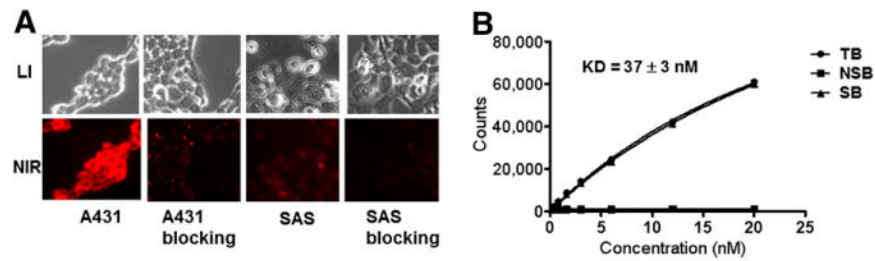
10. Orlova A, Feldwisch J, Abrahmsen L, Tolmachev V. Update: affibody molecules for molecular imaging and therapy for cancer. *Cancer Biother Radiopharm.* 2007; 22:573–584. [PubMed: 17979560]
11. Ahlgren S, Orlova A, Rosik D, et al. Evaluation of maleimide derivative of DOTA for site-specific labeling of recombinant affibody molecules. *Bioconjug Chem.* 2008; 19:235–243. [PubMed: 18163536]
12. Wikman M, Steffen AC, Gunneriusson E, et al. Selection and characterization of HER2/neu-binding affibody ligands. *Protein Eng Des Sel.* 2004; 17:455–462. [PubMed: 15208403]
13. Grönwall C, Snelders E, Palm AJ, Eriksson F, Herne N, Stahl S. Generation of Affibody ligands binding interleukin-2 receptor alpha/CD25. *Biotechnol Appl Biochem.* 2008; 50:97–112. [PubMed: 18284375]
14. Wikman M, Rowcliffe E, Friedman M, et al. Selection and characterization of an HIV-1 gp120-binding affibody ligand. *Biotechnol Appl Biochem.* 2006; 45:93–105. [PubMed: 16712522]
15. Engfeldt T, Orlova A, Tran T, et al. Imaging of HER2-expressing tumours using a synthetic Affibody molecule containing the  $^{99m}\text{Tc}$ -chelating mercaptoacetyl-glycyl-glycyl-glycyl (MAG3) sequence. *Eur J Nucl Med Mol Imaging.* 2007; 34:722–733. [PubMed: 17146656]
16. Kramer-Marek G, Kiesewetter DO, Martiniova L, Jagoda E, Lee SB, Capala J. [ $^{18}\text{F}$ ]FBEM-Z(HER2:342)-Affibody molecule-a new molecular tracer for in vivo monitoring of HER2 expression by positron emission tomography. *Eur J Nucl Med Mol Imaging.* 2008; 35:1008–1018. [PubMed: 18157531]
17. Namavari M, Padilla De Jesus O, Cheng Z, et al. Direct site-specific radiolabeling of an Affibody protein with 4- [ $^{18}\text{F}$ ]fluorobenzaldehyde via oxime chemistry. *Mol Imaging Biol.* 2008; 10:177–181. [PubMed: 18481153]
18. Orlova A, Magnusson M, Eriksson TL, et al. Tumor imaging using a picomolar affinity HER2 binding affibody molecule. *Cancer Res.* 2006; 66:4339–4348. [PubMed: 16618759]
19. Tolmachev V, Nilsson FY, Widstrom C, et al.  $^{111}\text{In}$ -benzyl-DTPA-ZHER2:342, an affibody-based conjugate for in vivo imaging of HER2 expression in malignant tumors. *J Nucl Med.* 2006; 47:846–853. [PubMed: 16644755]
20. Tran TA, Rosik D, Abrahmsen L, et al. Design, synthesis and biological evaluation of a multifunctional HER2-specific Affibody molecule for molecular imaging. *Eur J Nucl Med Mol Imaging.* 2009; 36:1864–1873. [PubMed: 19504093]
21. Ahlgren S, Orlova A, Wallberg H, et al. Targeting of HER2-expressing tumors using  $^{111}\text{In}$ -ABY-025, a second-generation affibody molecule with a fundamentally reengineered scaffold. *J Nucl Med.* 2010; 51:1131–1138. [PubMed: 20554729]
22. Friedman M, Orlova A, Johansson E, et al. Directed evolution to low nanomolar affinity of a tumor-targeting epidermal growth factor receptor-binding affibody molecule. *J Mol Biol.* 2008; 376:1388–1402. [PubMed: 18207161]
23. Nordberg E, Orlova A, Friedman M, et al. In vivo and in vitro uptake of  $^{111}\text{In}$ , delivered with the affibody molecule (ZEGFR:955)<sub>2</sub>, in EGFR expressing tumour cells. *Oncol Rep.* 2008; 19:853–857. [PubMed: 18357367]
24. Miao Z, Ren G, Liu H, Jiang L, Cheng Z. Small-animal PET imaging of human epidermal growth factor receptor positive tumor with a  $^{64}\text{Cu}$  labeled affibody protein. *Bioconjug Chem.* 2010; 21:947–954. [PubMed: 20402512]
25. Tolmachev V, Friedman M, Sandstrom M, et al. Affibody molecules for epidermal growth factor receptor targeting in vivo: aspects of dimerization and labeling chemistry. *J Nucl Med.* 2009; 50:274–283. [PubMed: 19164241]
26. Tolmachev V, Rosik D, Wallberg H, et al. Imaging of EGFR expression in murine xenografts using site-specifically labelled anti-EGFR  $^{111}\text{In}$ -DOTA-Z EGFR:2377 Affibody molecule: aspect of the injected tracer amount. *Eur J Nucl Med Mol Imaging.* 2010; 37:613–622. [PubMed: 19838701]
27. Baum RP, Prasad V, Muller D, et al. Molecular imaging of HER2-expressing malignant tumors in breast cancer patients using synthetic  $^{111}\text{In}$ - or  $^{68}\text{Ga}$ -labeled affibody molecules. *J Nucl Med.* 2010; 51:892–897. [PubMed: 20484419]

28. Miao Z, Ren G, Liu H, Jiang L, Cheng Z. Cy5.5-labeled Affibody molecule for near-infrared fluorescent optical imaging of epidermal growth factor receptor positive tumors. *J Biomed Opt.* 2010; 15:036007. [PubMed: 20615009]
29. Cai W, Zhang X, Wu Y, Chen X. A thiol-reactive  $^{18}\text{F}$ -labeling agent, N-[2-(4- $^{18}\text{F}$ -fluorobenzamido)ethyl]maleimide, and synthesis of RGD peptide-based tracer for PET imaging of alpha v beta 3 integrin expression. *J Nucl Med.* 2006; 47:1172–1180. [PubMed: 16818952]
30. Tang G, Zeng W, Yu M, Kabalka G. Facile synthesis of N-succinimidyl 4-[ $^{18}\text{F}$ ] fluorobenzoate ([ $^{18}\text{F}$ ]SFB) for protein labeling. *J Labelled Comp Radiopharm.* 2008; 51:68–71.
31. Ke S, Wen X, Gurfinkel M, et al. Near-infrared optical imaging of epidermal growth factor receptor in breast cancer xenografts. *Cancer Res.* 2003; 63:7870–7875. [PubMed: 14633715]
32. Jiang L, Miao Z, Kimura RH, et al. Preliminary evaluation of  $^{177}\text{Lu}$ -labeled knottin peptides for integrin receptor-targeted radionuclide therapy. *Eur J Nucl Med Mol Imaging.* 2011; 38:613–622. [PubMed: 21153409]
33. Cai W, Chen K, He L, Cao Q, Koong A, Chen X. Quantitative PET of EGFR expression in xenograft-bearing mice using  $^{64}\text{Cu}$ -labeled cetuximab, a chimeric anti-EGFR monoclonal antibody. *Eur J Nucl Med Mol Imaging.* 2007; 34:850–858. [PubMed: 17262214]
34. Nayak TK, Regino CA, Wong KJ, et al. PET imaging of HER1-expressing xenografts in mice with 86Y-CHX-A''-DTPA-cetuximab. *Eur J Nucl Med Mol Imaging.* 2010; 37:1368–1376. [PubMed: 20155263]
35. Cheng Z, De Jesus OP, Kramer DJ, et al.  $^{64}\text{Cu}$ -labeled affibody molecules for imaging of HER2 expressing tumors. *Mol Imaging Biol.* 2010; 12:316–324. [PubMed: 19779897]
36. Memon AA, Jakobsen S, Dagnaes-Hansen F, Sorensen BS, Keiding S, Nexø E. Positron emission tomography (PET) imaging with [ $^{11}\text{C}$ ]-labeled erlotinib: a micro-PET study on mice with lung tumor xenografts. *Cancer Res.* 2009; 69:873–878. [PubMed: 19155297]
37. Yeh HH, Ogawa K, Balatoni J, et al. Molecular imaging of active mutant L858R EGF receptor (EGFR) kinase-expressing nonsmall cell lung carcinomas using PET/CT. *Proc Natl Acad Sci USA.* 2011; 108:1603–1608. [PubMed: 21220318]
38. Cuartero-Plaza A, Martinez-Miralles E, Rosell R, Vadell-Nadal C, Farre M, Real FX. Radiolocalization of squamous lung carcinoma with  $^{131}\text{I}$ -labeled epidermal growth factor. *Clin Cancer Res.* 1996; 2:13–20. [PubMed: 9816084]
39. Liu S, Liu H, Jiang H, Xu Y, Zhang H, Cheng Z. One-step radiosynthesis of  $^{18}\text{F}$ -AIF-NOTA-RGD for tumor angiogenesis PET imaging. *Eur J Nucl Med Mol Imaging.* 2011; 38:1732–1741. [PubMed: 21617974]
40. Wu Z, Li ZB, Cai W, et al.  $^{18}\text{F}$ -labeled mini-PEG spaced RGD dimer ( $^{18}\text{F}$ -FPRGD2): synthesis and microPET imaging of alphavbeta3 integrin expression. *Eur J Nucl Med Mol Imaging.* 2007; 34:1823–1831. [PubMed: 17492285]



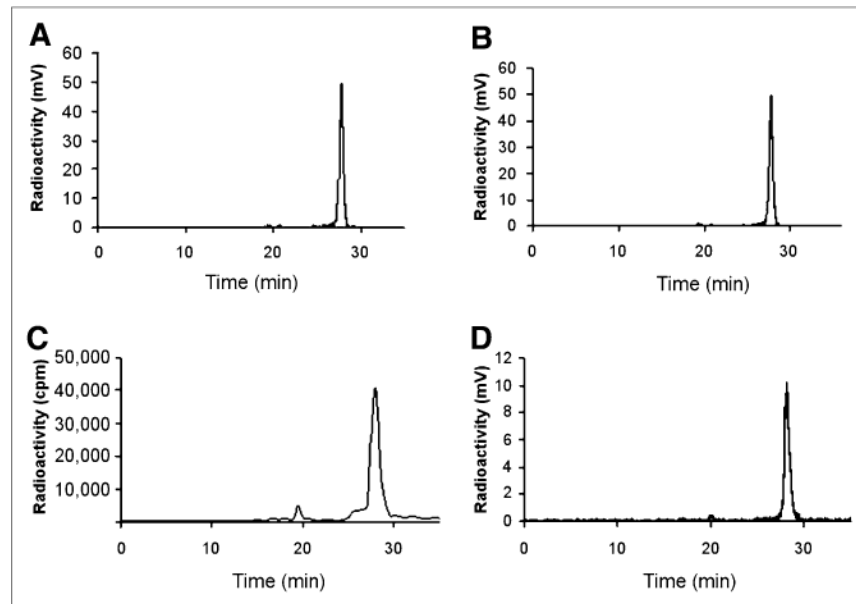
**FIGURE 1.**  
Scheme of radiosynthesis of  $^{18}\text{F}$ -FBEM-Cys-Z<sub>EGFR:1907</sub>.



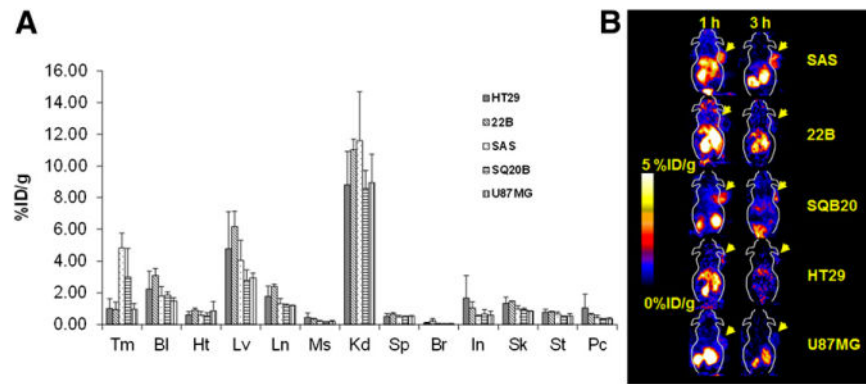


**FIGURE 2.**

(A) Competitive binding of Ac-Cys-Z<sub>EGFR:1907</sub> to EGFR with Cy5.5-EGF. (B) Binding affinity assay of <sup>18</sup>F-FBEM-Cys-Z<sub>EGFR:1907</sub> using EGFR-positive A431 cells. LI = white light; NIR = near-infrared; NSB = nonspecific binding; TB = total binding; SB = specific binding.



**FIGURE 3.** In vitro stability assay of  $^{18}\text{F}$ -FBEM-Cys-Z<sub>EGFR:1907</sub> after incubation in mouse serum for 1 (A) and 3 (B) h. In vivo stability assay of  $^{18}\text{F}$ -FBEM-Cys-Z<sub>EGFR:1907</sub> from samples of plasma (C) and tumor (D) at 1 h after injection.

**FIGURE 4.**

(A) Biodistribution of  $^{18}\text{F}$ -FBEM-Cys- $Z_{\text{EGFR}:1907}$  at 3 h after injection in EGFR overexpression xenograft models ( $n = 3$ ). (B) Representative  $^{18}\text{F}$ -FBEM-Cys- $Z_{\text{EGFR}:1907}$  PET of tumor xenograft models with EGFR overexpression. Bl = blood; Br = brain; Ht = heart; In = intestine; Kd = kidney; Lv = liver; Ln = lungs; Ms = muscle; Pc = pancreas; Sk = skin; Sp = spleen; St = stomach; Tm = tumor.

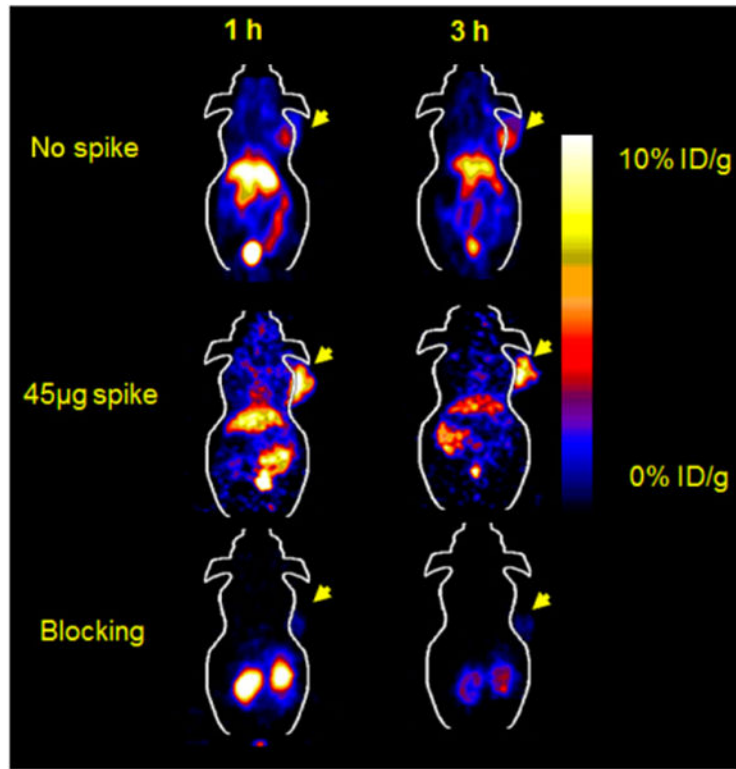


**FIGURE 5.** Small-animal PET of  $^{18}\text{F}$ -FBEM-Cys-Z<sub>EGFR:1907</sub> in A431 xenograft model coinjected with 0, 45, and 500 µg (blocking dose) of Ac-Cys-Z<sub>EGFR:1907</sub>.

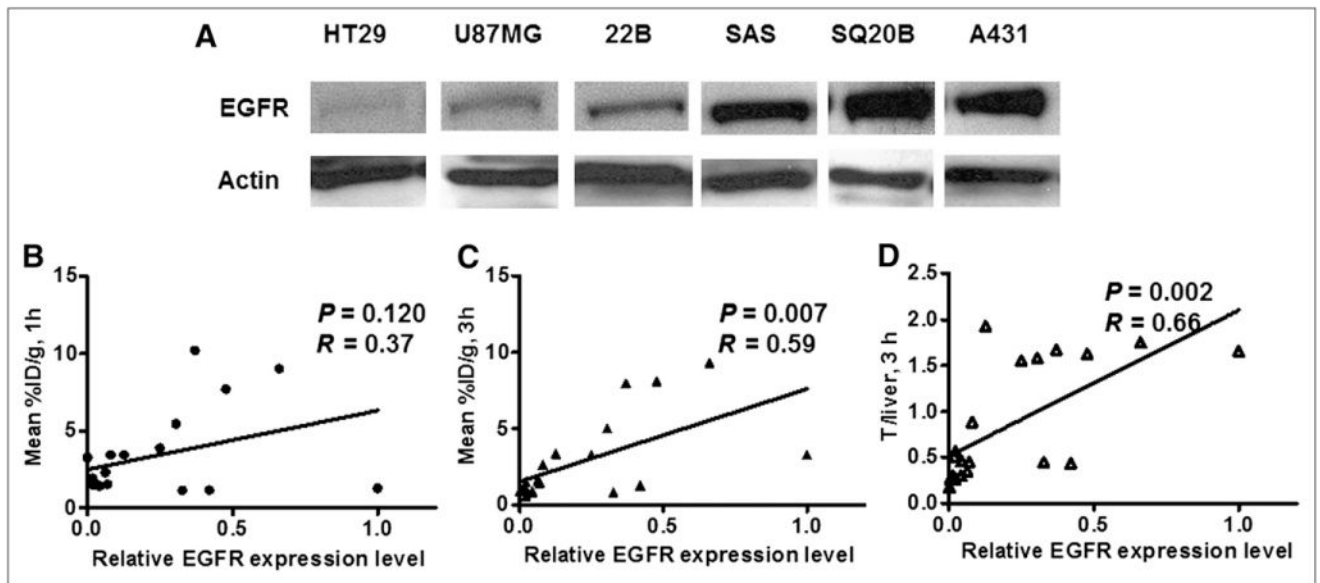


**FIGURE 6.**

(A) Western blot quantification of EGFR expression at various tumor xenograft models. Correlation of PET quantification of tumor uptake at 1 h after injection (B) or 3 h after injection (C), or tumor-to-liver uptake ratio at 3 h after injection (D) with normalized EGFR expression level ( $n = 19$ ).

TABLE 1

Biodistribution of  $^{18}\text{F}$ -FBEM-Cys-Z<sub>EGFR</sub>:1907 in Nu/v-Mice Bearing Subcutaneously Xenotransplanted A431 with Spiked Dose (Ac-Cys-Z<sub>EGFR</sub>:1907)

Organ	Dose ( $\mu\text{g}$ )		
	0	45	500, block
Tumor	$3.94 \pm 0.39$ <sup>†</sup>	$8.06 \pm 1.44$ <sup>†*</sup>	$0.97 \pm 0.42$ <sup>*</sup>
Blood	$3.75 \pm 0.12$ <sup>†</sup>	$3.12 \pm 0.10$ <sup>†*</sup>	$0.12 \pm 0.03$ <sup>*</sup>
Heart	$0.79 \pm 0.04$	$0.71 \pm 0.05$ <sup>*</sup>	$0.06 \pm 0.02$ <sup>*</sup>
Liver	$9.28 \pm 1.61$ <sup>†</sup>	$6.50 \pm 0.31$ <sup>†*</sup>	$0.33 \pm 0.15$ <sup>*</sup>
Lungs	$1.54 \pm 0.10$	$1.87 \pm 0.32$ <sup>*</sup>	$0.14 \pm 0.07$ <sup>*</sup>
Muscle	$0.32 \pm 0.05$	$0.23 \pm 0.05$ <sup>*</sup>	$0.02 \pm 0.01$ <sup>*</sup>
Kidney	$3.78 \pm 0.36$ <sup>†</sup>	$4.75 \pm 0.14$ <sup>†</sup>	$6.14 \pm 2.87$
Spleen	$0.61 \pm 0.03$	$0.51 \pm 0.07$ <sup>*</sup>	$0.15 \pm 0.07$ <sup>*</sup>
Brain	$0.18 \pm 0.07$	$0.14 \pm 0.01$ <sup>*</sup>	$0.01 \pm 0.01$ <sup>*</sup>
Intestine	$1.02 \pm 0.27$	$0.75 \pm 0.14$ <sup>*</sup>	$0.37 \pm 0.37$ <sup>*</sup>
Skin	$1.12 \pm 0.48$	$1.10 \pm 0.10$ <sup>*</sup>	$0.08 \pm 0.05$ <sup>*</sup>
Stomach	$1.16 \pm 0.14$ <sup>†</sup>	$0.71 \pm 0.10$ <sup>*</sup>	$0.06 \pm 0.03$ <sup>*</sup>
Pancreas	$0.56 \pm 0.42$	$0.52 \pm 0.02$ <sup>*</sup>	$0.04 \pm 0.01$ <sup>*</sup>
Bone	$0.31 \pm 0.23$	$0.41 \pm 0.09$ <sup>*</sup>	$0.12 \pm 0.04$ <sup>*</sup>
Uptake ratio			
Tumor to blood	$1.05 \pm 0.08$ <sup>†</sup>	$2.58 \pm 0.47$ <sup>†*</sup>	$7.76 \pm 1.29$ <sup>*</sup>
Tumor to lung	$2.56 \pm 0.120$	$4.32 \pm 0.35$ <sup>†*</sup>	$7.26 \pm 0.43$ <sup>*</sup>
Tumor to muscle	$12.80 \pm 3.32$ <sup>†</sup>	$36.88 \pm 12.77$ <sup>†</sup>	$40.29 \pm 2.70$

\*  $P < 0.05$ , comparison of biodistribution between probe spiked with 45 and 500  $\mu\text{g}$  (blocking dose) of Ac-Cys-Z<sub>EGFR</sub>:1907 at 3 h after injection.

<sup>†</sup>  $P < 0.05$ , comparison of biodistribution between probe spiked with 0 and 45  $\mu\text{g}$  of Ac-Cys-Z<sub>EGFR</sub>:1907 at 3 h after injection.

Data are mean  $\pm$  SD, expressed as percentage administered activity (injected probe) per gram of tissue (%ID/g) after intravenous injection of probe (1.85–2.59 MBq [50–70  $\mu\text{Ci}$ ], ~2–3  $\mu\text{g}$ ) spiked with 0, 45, and 500  $\mu\text{g}$  of Ac-Cys-Z<sub>EGFR</sub>:1907 at 3 h after injection. Significant inhibition of  $^{18}\text{F}$ -FBEM-Cys-Z<sub>EGFR</sub>:1907 uptake was observed in A431 tumor of blocked group (500  $\mu\text{g}$ ) ( $P < 0.05$ ).